ELSEVIER

Journal of Molecular Catalysis A: Chemical 163 (2000) 283–296

JOURNAL OF MOLECULAR CATALYSIS A: CHEMICAL

www.elsevier.com/locate/molcata

Metastable fcc α-MoC_{1-x} supported on HZSM5: preparation and catalytic performance for the non-oxidative conversion of methane to aromatic compounds

C. Bouchy [a], I. Schmidt [a,b], J.R. Anderson [a], C.J.H. Jacobsen [b], E.G. Derouane [a], S.B. Derouane-Abd Hamid [a,*]

[a] *Department of Chemistry, Leverhulme Center for Innovative Catalysis, University of Liverpool, P.O. Box 147, Liverpool, L69 3BX, UK*

[b] *Haldor Topsøe Research Laboratories, Haldor Topsøe A/S, Nymøllevej 55, DK-2800 Lyngby, Denmark*

Received 10 June 2000; accepted 20 July 2000

Abstract

There exist two forms of molybdenum carbide: the stable hexagonally close packed (hcp) structure β-Mo_2C and the metastable face centered cubic (fcc) structure α-MoC_{1-x}. Bulk fcc α-MoC_{1-x} can be prepared by controlled preactivation in hydrogen or hydrogen/hydrocarbon mixtures, at moderate temperature (623 K), of MoO_3. Fcc structure molybdenum oxyhydride or molybdenum oxycarbide are initially formed, respectively, by a topotactic transformation and they can be further carburized to yield fcc α-MoC_{1-x}. However, zeolite-supported α-MoC_{1-x} cannot be prepared by this route when hydrogen is used, probably as a result of MoO_3-zeolite interactions or a too small size of the MoO_3 crystals which facilitate the reduction of MoO_3 to MoO_2. Carbon stabilization, leading to the fcc structure oxycarbide is necessary, which can be achieved by activating MoO_3 with a hydrogen/*n*-butane mixture at 623 K. The latter is then easily carburized to yield fcc α-MoC_{1-x}. Molybdenum carbide species were identified to be active components in Mo-modified catalysts used for the direct dehydroaromatization of methane. The catalytic performance of HZSM5 modified by either hcp β-Mo_2C, the classical catalyst well described in the literature, and fcc α-MoC_{1-x}, the new catalytic system we prepared, have been compared. The latter shows superior performance: higher activity, higher selectivity to benzene, and higher stability as a function of time-on-stream.

Keywords: Catalysis; Zeolites; Transition metal carbides; Methane activation; Methane upgrading; Molybdenum carbide

1. Introduction

In 1973, Levy and Boudart reported that transition metal carbides, e.g. W and Mo carbides, may show catalytic properties resembling those of noble metals [1]. Their original report triggered many investigations on transition metal interstitial compounds (carbides, oxycarbides, nitrides, and oxynitrides) [2] because of their potential for the replacement of noble metals in catalysts. In particular, interstitial compounds of metals from group V to VI (V, W, Mo) were studied extensively as they appeared to catalyse several important reactions [3–6].

There exist two molybdenum carbide phases: the thermodynamically stable phase, β-Mo_2C, whose

* Corresponding author. Tel.: +44-151-794-2397; fax: +44-151-794-3589.
E-mail address: sharifhd@liverpool.ac.uk (S.B. Derouane-Abd Hamid).

1381-1169/00/$ – see front matter
PII: S1381-1169(00)00392-7

structure is hexagonally close packed (hcp), and the metastable phase, α-MoC_{1-x}, whose structure is face centered cubic (fcc). Both compounds were tested as catalysts for hydrotreating reactions, e.g. hydrodesulfurization [7] and hydrodenitrogenation [8–10], showing that these molybdenum carbides had catalytic performances comparable with that of commercial hydrotreating catalysts. Interestingly, Ranhotra found that the α and β molybdenum carbide phases exhibit different catalytic properties for the hydrogenolysis of ethane [11].

In most cases, earlier catalytic tests were performed using unsupported carbide powders, except for β-Mo_2C which, in some cases, was dispersed on a support, either alumina [12] or silica [13]. To our knowledge, the preparation and catalytic evaluation of supported α-MoC_{1-x} catalyst has not been reported.

β-Mo_2C with specific surface areas in 50–100 $m^2\,g^{-1}$ range can be prepared by temperature programmed reduction and carburization of MoO_3, using methane or a hydrogen/methane mixture [14]. The preparation of α-MoC_{1-x} with a specific surface area of about 200 $m^2\,g^{-1}$ has been reported via two different routes: (i) a two-step process comprising the initial nitridation of MoO_3 by ammonia followed by carburization of the γ-Mo_2N nitride [15] and (ii) a one-step process involving the direct carburization of MoO_3 impregnated with platinum [16]. We reported recently that the direct carburization of MoO_3 reduced to the Mo-oxyhydride by hydrogen at 623 K also yields the fcc carbide α-MoC_{1-x} [17]. This method presents two advantages: (i) the carbide is not contaminated with platinum traces that might affect its catalytic behavior and (ii) the use of ammonia is avoided. The latter fact is very relevant to the preparation of α-MoC_{1-x} supported on acidic zeolites because exposure of zeolites to ammonia at high temperature may result in structural damage [18].

Since Wang et al. [19] reported that methane could be dehydrocyclized to aromatic products (naphthalene, toluene, methyl-naphthalene, etc.) and hydrogen, at 973 K in non-oxidative conditions, using a Mo-modified HZSM5 zeolite, this reaction has received increased attention as it is a potential route to add value to methane, a relatively cheap and abundant raw material, yielding both aromatic hydrocarbons, that are widely used in the petrochemical and chemical sectors, and large amounts of hydrogen (ca. 9 mol of hydrogen per mol of aromatic compound produced).

It is now generally accepted that the active molybdenum-containing phase in the active catalyst is a carbide, β-Mo_2C, formed during an induction period when the Mo-modified zeolite precursor is reduced by exposure to methane under reaction conditions [20]. With a single exception, a report by our group [21], all results in the current literature can be attributed to HZSM5 supported β-Mo_2C catalysts.

One of the main challenges to improve the performance of such catalysts is increasing their lifetime, essentially by reducing the rate of catalyst deactivation due to coking, a difficult task when large amounts of heavy aromatic compounds are produced at high temperature.

This study describes a route for the preparation of bulk α-MoC_{1-x} and its application to the preparation of α-MoC_{1-x}/HZSM5 catalysts. It further demonstrates that a catalyst consisting of α-MoC_{1-x} supported on HZSM5 has superior properties for the direct, non-oxidative, conversion of methane to liquid aromatic products. The catalyst lifetime is dramatically increased and the benzene to naphthalene ratio in the products is about doubled.

2. Experimental

2.1. Carburization of bulk MoO_3

MoO_3 (300 mg, Mdrich, analytical grade) was activated at 623 K under hydrogen (30 ml min^{-1}) or under a hydrogen/*n*-butane mixture (v/v = 11/1, 30 ml min^{-1}) for 24 h. The gas flow was then switched to pure methane (16 ml min^{-1}) and the temperature raised to 983 K at a rate of 3 K min^{-1}. This treatment has been reported to yield α-MoC_{1-x} [17,21].

The same MoO_3 precursor was also directly carburized under methane only. For this purpose, MoO_3 was heated under helium (50 ml min^{-1}) up to 623 K at a rate of 20 K min^{-1}. The gas flow was then switched to methane only (16 ml min^{-1}) and the temperature increased to 983 K at a rate of 3 K min^{-1}. This treatment has been shown to yield β-MO_2C [14].

The structural transformations occurring during these treatments were followed by in situ powder X-ray diffraction (XRD). Scanning electron microscopy

(SEM) was also used to characterize the morphology of selected products.

2.2. Preparation of Mo-modified zeolite HZSM5 (Mo/HZSM5)

HZSM5 was obtained by calcining NH_4-ZSM5 (Zeolyst International, batch CBV 80140G, $SiO_2/Al_2O_3 = 80$) at 773 K for 4 h. A Mo/HZSM5 precursor containing 10 wt.% of MoO_3 was prepared by wet impregnation of HZSM5 with an aqueous solution of ammonium heptamolybdate ($(NH_4)_6[Mo_7O_{24}]\cdot 4H_2O$, Aldrich, analytical grade) as described previously [21]. The dried precursor was calcined in situ at 673 K in air for 1 h prior to further activation.

2.3. Preparation of HZSM5-supported β-Mo_2C

In situ calcined sample was activated by a hydrogen/methane mixture (v/v = 11/1, total 63 ml min^{-1}). The temperature was ranged from 298 to 973 K at a rate of 5 K min^{-1}. The gas mixture was then switched to pure methane (16.7 ml min^{-1}) and the temperature was held at 973 K for 10 min.

2.4. Preparation of HZSM5-supported α-MoC_{1-x}

The in situ calcined sample was activated in hydrogen (63 ml min^{-1}) or a hydrogen/*n*-butane mixture (v/v = 11/1, total = 63 ml min^{-1}) for 24 h. The temperature was ranged from 298 to 623 K at a rate of 16 K min^{-1}, held at 623 K for 24 h, and then cooled to 298 K. The sample was not cooled before further carburization, but treated as described below.

The sample obtained by the above activation treatments was carburized in a hydrogen/*n*-butane gas mixture (v/v = 11/1, total 63 ml min^{-1}). The temperature was ranged from 623 to 823 K at a rate of 5 K min^{-1}. At 823 K, the gas mixture was switched to pure methane (16.7 ml min^{-1}) and the temperature ranged to 973 K at a rate of 5 K min^{-1}. These conditions were maintained for 10 min.

2.5. Catalyst characterization: XRD, SEM, and TEM

For in situ powder XRD experiments, a Siemens D5005 diffractometer (θ–2θ mode, Cu Kα radiation) was equipped with a Paar in situ cell and a position sensitive detector enabling the fast acquisition (<6 min) of XRD patterns. In situ diffractograms were recorded over 2θ values ranging from 10 to 60° with a scanning rate of 0.1 s per step and a step size of 0.0144°. The various gases (hydrogen, helium, methane and *n*-butane) were introduced in the Paar cell using a set of mass flow controllers (Brooks, 5850TR) previously calibrated. Ex situ diffractograms were recorded over 2θ values ranging from 15 to 60° with a scanning rate of 0.02 s per step. Both molybdenum carbide regions were further analyzed in more detail in 30–50° (2θ) range at a scanning rate of 5 s per step. Transmission electron microscopy (TEM) and selected area diffraction (SAD) characterizations were performed on a JEOL 2000 FX instrument operating at 200 kV with a spot size of 0.5 μm. For the analyses, the sample was ground with a mortar and pestled, and some dried powder layered on a holy-carbon coated grid. The SEM characterization of the powder samples was performed using a HITACHI S2460N instrument in the secondary electron imaging mode at 20 kV. Prior to insertion, the powder samples were sprinkled onto AGAR carbon conductor tabs adhering to conventional SEM stubs.

2.6. Catalytic microreactor tests

Samples were tested towards their catalytic performance for the direct dehydrocyclization of methane (16.7 ml min^{-1}) to aromatics following in situ pre-treatments described above. Testing was performed at atmospheric pressure using a fixed bed continuous plug-flow microreactor system consisting of an 11 mm-i.d. 316 stainless steel reactor tube containing ca. 1 g of catalyst, plugged at both ends with quartz wool. The reaction temperature (973 K) was monitored using a K-type thermocouple positioned in the catalyst bed and gas flows were monitored and regulated with Brooks 5850S mass flow controllers. The outlet of the reactor was kept above 500 K to avoid condensation of heavy hydrocarbons. On-line analysis of the effluent was performed with a Varian Star 3400CX gas chromatograph using the Varian Star 4.5 data handling software. The aromatic products were separated using a capillary HP-1 column and quantified using an FID detector. Other products were

separated using a Porapak Q column and detected using a TCD detector.

2.7. Direct carburization of bulk MoO_3: preparation of bulk β-Mo_2C

Fig. 1 shows the changes occurring in the XRD pattern, measured in situ under methane flow in the temperature of 863–983 K range.

A qualitative description of the reduction–carburization process can be obtained by plotting the relative intensity of a diffraction peak characteristic of each crystalline phase as a function of temperature (Fig. 2). MoO_3 is slowly reduced to MoO_2 between 700 and 863 K. Rapid reduction of MoO_3 to MoO_2 starts at 863 K and it is accompanied by the formation of the intermediate suboxide Mo_4O_{11}. MoO_2 is the only major phase present at 923 K. Its complete carburization yielding β-Mo_2C takes place between 953 and 983 K. Scheme 1 summarizes the transformation pathway.

The SEM picture of MoO_3 before and after carburization (Fig. 3, direct carburization) shows that the

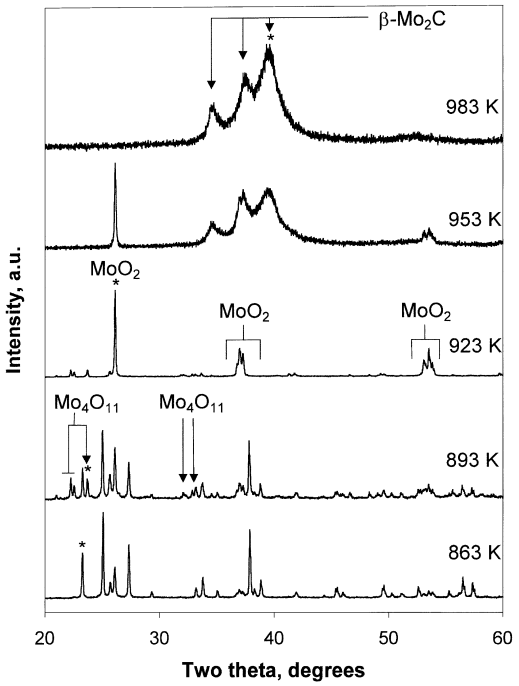

Fig. 1. In situ XRD patterns recorded during the direct carburization of bulk MoO_3 by methane in the temperature of 863–983 K range. MoO_3 peaks are not indexed.

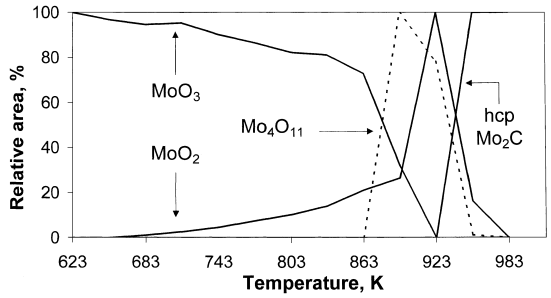

Fig. 2. Evolution of the relative intensity of a diffraction peak characteristic of each crystalline phase during the direct carburization of unsupported MoO_3 by methane. The selected diffraction peaks are identified by a '*' in Fig. 1.

platelet morphology of the parent oxide, typical of a layered compound, is lost after carburization. β-Mo_2C appears as aggregates of small 1–2 μm crystals with poorly defined shapes.

2.8. Carburization of bulk MoO_3 after activation at 623 K: preparation of bulk α-MoC_{1-x}

2.8.1. Activation of bulk MoO_3 at 623 K

XRD patterns of MoO_3 after in situ activation at 623 K under pure hydrogen or hydrogen/*n*-butane are shown in Fig. 4. As reported [22], the activation of MoO_3 with hydrogen/*n*-butane leads to the formation of two compounds, MoO_2 and a molybdenum oxycarbide, $MoO_{x'}H_{y'}C_z$. This oxycarbide has a fcc structure with a unit cell length of 0.410 nm and a stoichiometry estimated to be $MoO_{2.42}C_{0.23}H_{0.78}$ [23]. A similar pattern is observed when MoO_3 is activated under hydrogen only. It shows the formation of MoO_2 and molybdenum oxyhydride, MoO_xH_y. The latter is isostructural with the oxycarbide [23]. Both the oxyhydride and the oxycarbide are obtained from MoO_3 through a topotactic transformation, and the insertion of hydrogen into the oxide was identified as the key point of their syntheses [24,25]. The presence of carbon and hydrogen in the oxycarbide has been quantified by temperature programmed oxidation (TPO) and temperature programmed desorption measurements [24,26].

$$MoO_3 \rightarrow Mo_4O_{11} \rightarrow MoO_2 \rightarrow \beta\text{-}Mo_2C$$

Scheme 1.

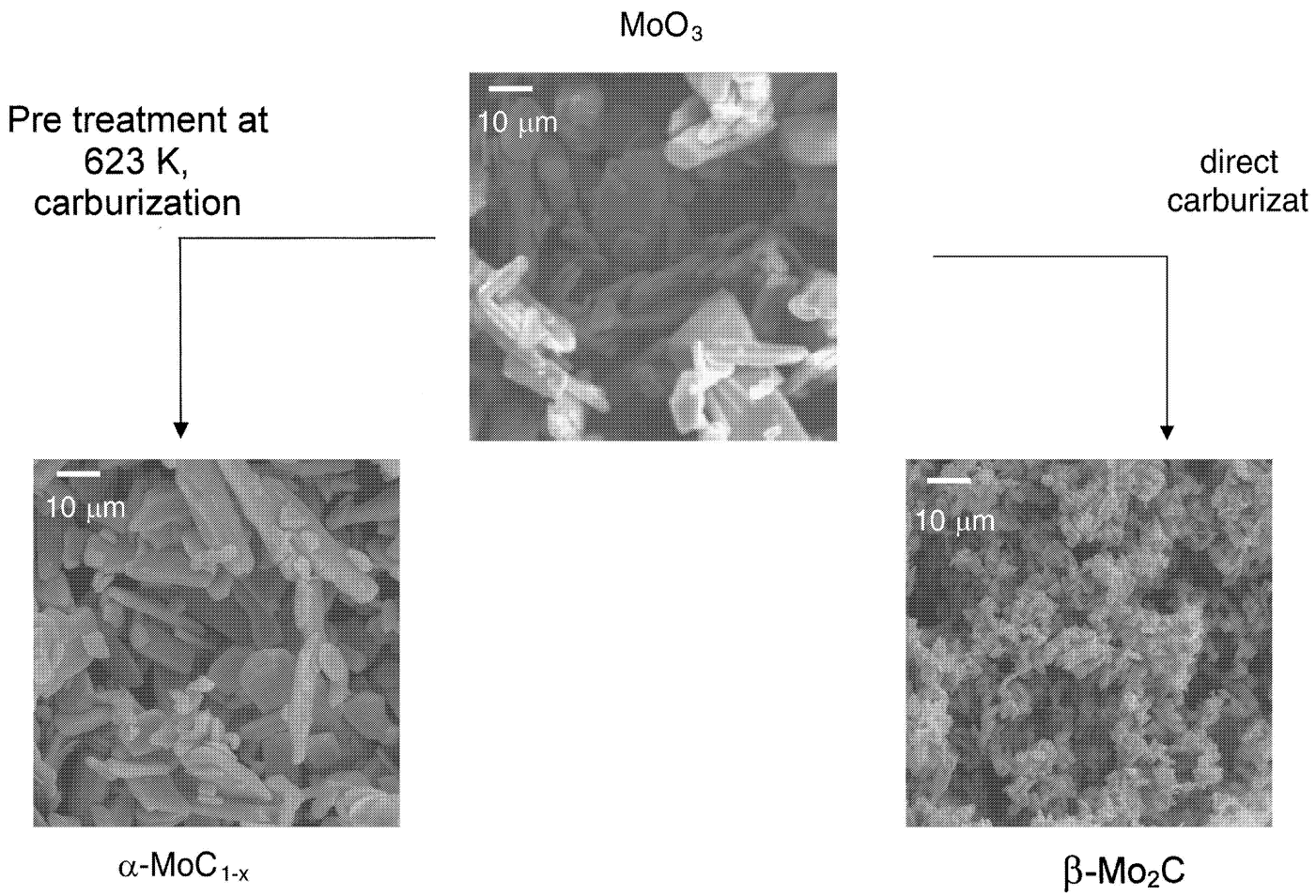

Fig. 3. SEM pictures showing the morphologies of MoO_3, α-MoC_{1-x} and β-Mo_2C.

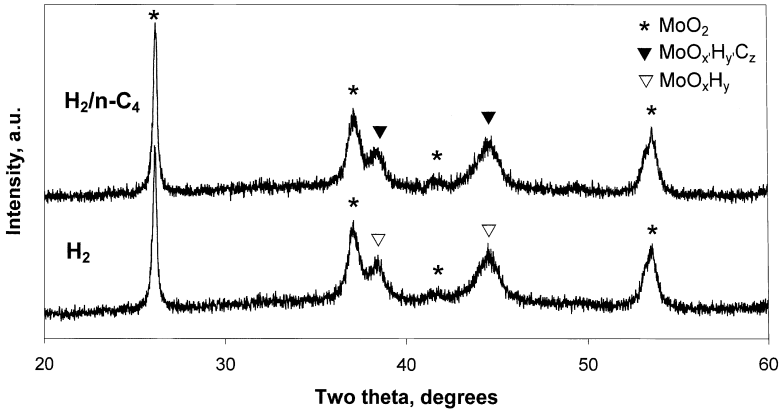

Fig. 4. XRD patterns of MoO_3 after activation at 623 K under hydrogen or a hydrogen/*n*-butane mixture.

2.8.2. Carburization of bulk MoO_3 activated at 623 K under hydrogen

In situ XRD was used to follow the carburization of bulk MoO_3 activated at 623 K under hydrogen, i.e. a mixture of MoO_xH_y and MoO_2, in the temperature of 623–983 K range and using methane only. Up to 863 K, the diffraction peaks of MoO_2 and MoO_xH_y remained unchanged, showing that bulk carburization of neither phase was occurring. Fig. 5 shows the transformations occurring in the temperature of 863–983 K range. At 893 K, part of the sample has been carburized, mostly to α-MoC_{1-x} and at the expense of the oxyhydride phase. The latter phase was completely carburized at 923 K whereas some MoO_2 was still present. Full carburization of the sample was achieved at 953 K, yielding α-MoC_{1-x} as the main carbide phase with only traces of β-Mo_2C. Similar transformations were observed during the carburization by methane of the $MoO_{x'}H_{y'}C_z$–MoO_2 mixture obtained by activation of bulk MoO_3 with a hydrogen/*n*-butane mixture.

As the carburization of MoO_2 under similar conditions leads to the formation of β-Mo_2C; the formation of the fcc α-MoC_{1-x} carbide can be unambiguously attributed to the carburization of either the fcc oxyhydride or the fcc oxycarbide. Traces of β-Mo_2C in the final material imply that only a small amount of MoO_2 is formed after the activation treatment at 623 K. Scheme 2 summarizes the successive transformations that occurred.

The unit cell length of the fcc α-MoC_{1-x} carbide is $a_{cub} = 0.428$ nm and its stoichiometry, estimated previously, $MoC_{0.7}$ [17]. The value of a_{cub} confirms that a pure carbide and not an oxycarbide is formed, the various oxycarbides being characterized by lower a_{cub} values [24,27] and this carbide is similar to the one previously described in the literature [28]. The coherent X-ray domain size calculated from the broadening

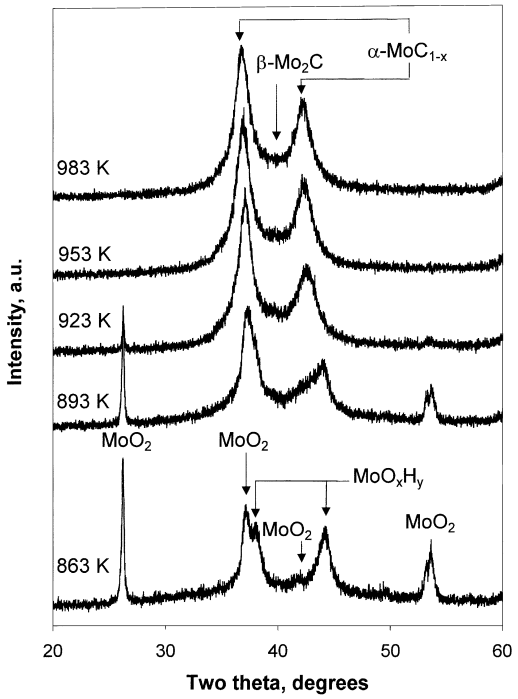

Fig. 5. In situ XRD patterns recorded during the carburization of bulk MoO_xH_y–MoO_2 by methane.

$$MoO_3 \longrightarrow \underset{(MoO_2,\ \text{traces})}{MoO_xH_y \text{ or } MoO_xH_yC_z} \longrightarrow \underset{(\beta\text{-}Mo_2C,\ \text{traces})}{\alpha\text{-}MoC_{1-x}}$$

Scheme 2.

of the XRD pattern using Scherrer's equation is ca. 3.4 nm.

SEM pictures of MoO_3 before and after carburization by this two-step route are shown in Fig. 3. The shape of the parent oxide particles is retained in α-MoC_{1-x}, implying that the transformation process is pseudomorphous, which is often characteristic of a topotactic transformation. This is in contrast to the synthesis of β-Mo_2C. As the size of the coherent X-ray domains is much smaller that the particle size (in the micron range), a nucleation-growth mechanism is probably also involved in this transformation.

TEM and SAD characterizations (Fig. 6) of α-MoC_{1-x} confirm that the route from MoO_3 to α-MoC_{1-x} is topotactic according to the Oswald and Günter definition [29]. SAD performed on the basal plane of a particle of α-MoC_{1-x} shows a diffraction pattern matching that of an fcc structure (a_{cub} = 0.428 nm) and the axis zone is $\langle 1\,0\,0\rangle$. It implies that all the α-MoC_{1-x} carbide diffracting domains have the same orientation. As the basal plane of the initial particle (MoO_3) was the (0 k 0) plane of MoO_3, the $\langle 1\,0\,0\rangle$ direction of the α-MoC_{1-x} crystallites is concluded to be parallel to the $\langle 0\,1\,0\rangle$ direction of the MoO_3 crystallites. The observation of relatively large electron diffraction spots confirms the small size of the diffraction domains/crystallites estimated from the XRD measurements.

2.9. Preparation of zeolite-supported carbides

Supported molybdenum carbides were prepared using a Mo (10 wt.%) modified HZSM5 zeolite precursor. Studying the carburization of MoO_3 using such a system is complicated by three factors: (i) the lower concentration of Mo-containing species; (ii) the broadening of the Mo-containing species diffraction peaks due to their high dispersion and (iii) possible interference with diffraction peaks arising from the zeolite.

The XRD patterns of the precursor activated at 623 K using a hydrogen/*n*-butane mixture (a) or hydrogen only (b) are compared with the XRD pattern of the calcined precursor (c) in Fig. 7. The pattern of the calcined sample (c) shows the formation of MoO_3 and HZSM5. No MoO_3 is detected by XRD in the activated samples, implying that MoO_3

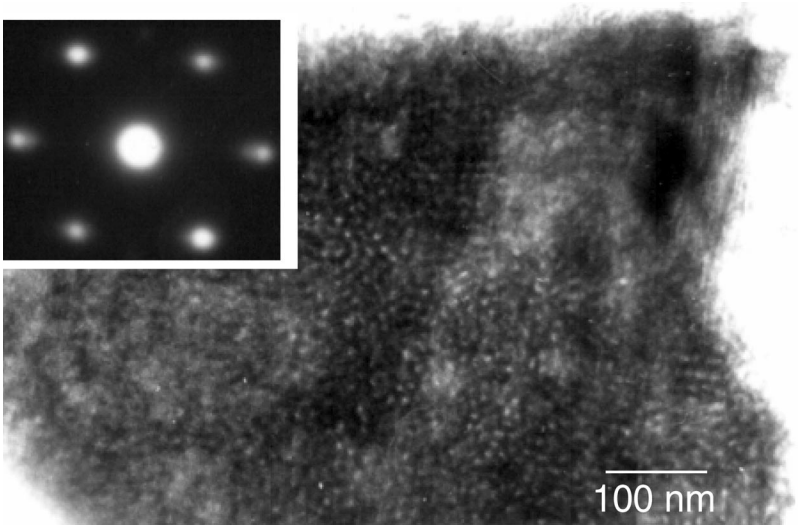

Fig. 6. TEM and SAD characterizations of α-MoC_{1-x}.

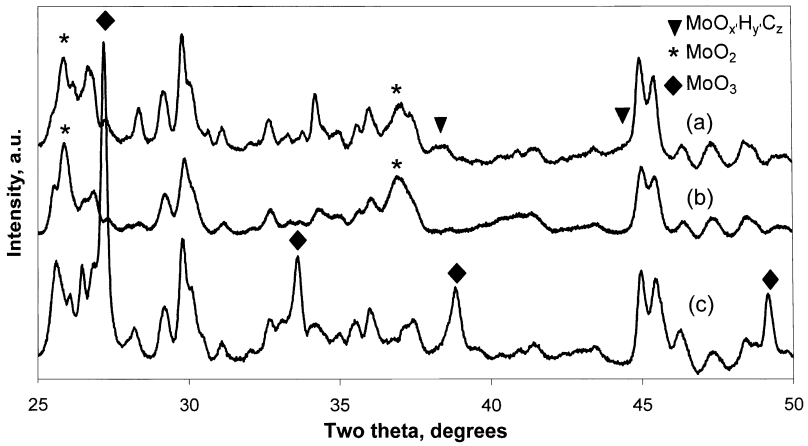

Fig. 7. XRD patterns of the calcined precursor, MoO_3/HZSM5, and of materials obtained after treatment at 623 K: (a) sample activated under hydrogen/*n*-butane; (b) sample activated under hydrogen; (c) MoO_3/HZSM5. HSZM5 peaks are not indexed.

has been entirely converted to other Mo-containing phases during activation. Broad reflections at an angle $2\theta = 26.1$ and 37.2° for the sample activated in hydrogen (b) are consistent with the presence of MoO_2. By contrast, when the sample is activated using a hydrogen/*n*-butane mixture (c), the amount of MoO_2 is very much reduced and is at or below the XRD detection sensitivity. Instead, the presence of $MoO_{x'}H_{y'}C_z$ is indicated by the presence of a new broad but distinct diffraction peak at $2\theta = 38.5^\circ$ and a weak shoulder at the left of a zeolite diffraction peak at $\theta = 44.6^\circ$.

The XRD patterns obtained after carburization of the (a) and (b) samples mentioned above by methane are shown in Fig. 8. After carburization, the hydrogen-activated sample shows the presence of hcp β-Mo_2C ($2\theta = 34.7$, 37.8 and 39.7°) only and no fcc α-MoC_{1-x}. By contrast, no hcp β-Mo_2C is detected after carburization of the sample activated in hydrogen/*n*-butane. Instead, broad peaks at $2\theta = 36.5$ and 42° are observed, which indicate the presence of fcc α-MoC_{1-x}.

The above observations are of major importance. They show that fcc α-MoC_{1-x} can be formed from

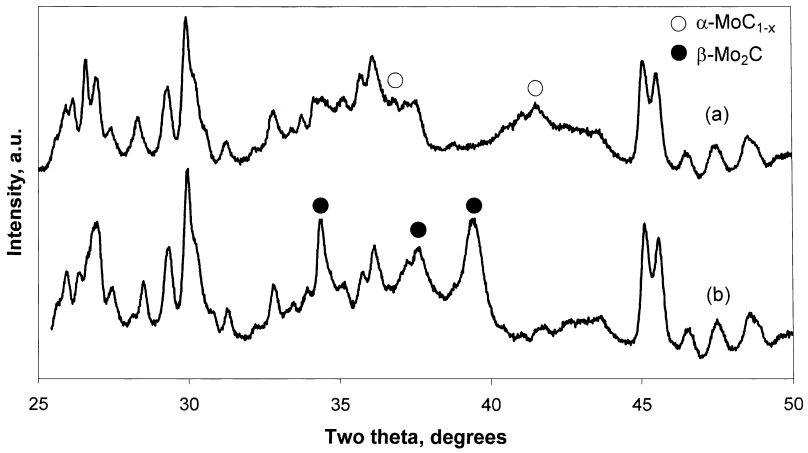

Fig. 8. XRD patterns of the carburized samples: (a) sample activated under hydrogen/*n*-butane and carburized with methane; (b) sample activated under hydrogen and carburized with methane. HSZM5 peaks are not indexed.

bulk MoO_3 by activation under either hydrogen or hydrogen/*n*-butane followed by carburization under methane, whereas it can only be formed from zeolite-supported MoO_3 when hydrogen/*n*-butane activation is used. They also show that the molybdenum oxyhydride is not formed when reducing zeolite-supported MoO_3 under hydrogen. Both facts point out to the important role played by carbon in stabilizing the fcc structure of the oxycarbide.

2.10. Catalytic microreactor aromatization of methane

Two samples, consisting of HZSM5 zeolite-supported β-Mo_2C (prepared as described in Section 2) and α-MoC_{1-x}, respectively, were used as catalysts for the aromatization of methane at 973 K and atmospheric pressure using a conventional fixed-bed plug-flow reactor.

The samples were calcined in air at 873 K, instead of 673 K as part of the in situ activation procedure, which should not affect the following observations in view of the XRD results reported above. Conversions and selectivities (without accounting for coke formation) are expressed on a carbon basis. Zero hour time-on-stream is defined as the time when the temperature reached 973 K. Rates of formation of the products are calculated using methane conversions, products selectivities, total gaseous flow and are expressed on a carbon basis in nmol s^{-1}.

Fig. 9 compares the activities of both catalysts as a function of reaction time whereas Fig. 10 compares their selectivities towards benzene, naphthalene and C_2's. β-Mo_2C/HZSM5 showed a maximum conversion of ca. 5% after 2 h, the conversion then decreased steadily to reach only 2.5% after 25 h on stream. In contrast, the conversion observed for α-MoC_{1-x}/HZSM5 increased somewhat more slowly, initially, but remained constant at ca. 6% after 5 h. It is also most interesting to note that the α-MoC_{1-x}/HZSM5 catalyst is more selective towards the production of benzene than the β-Mo_2C/HZSM5 catalyst. In both cases, benzene/naphthalene ratios remained nearly constant throughout the test and were 4 and 2, respectively, which may explain the higher stability of the α-MoC_{1-x}/HZSM5 catalyst as a function of time-on-stream. Indeed, polyaromatic hydrocarbons are known to be efficient coke precursors.

Fig. 11 shows the evolution with reaction time of the rates of formation of aromatic and C_2 compounds for both catalysts. The variations in the formation rates of aromatic compounds (benzene, toluene, naphthalene and methylnaphthalene) parallel variations in conversion, indicating that the primary reaction is indeed the formation of aromatic compounds. The rates of formation of C_2-species (ethane and ethylene) are much lower and comparable for both catalysts, with only a small increase as function of time-on-stream being observed.

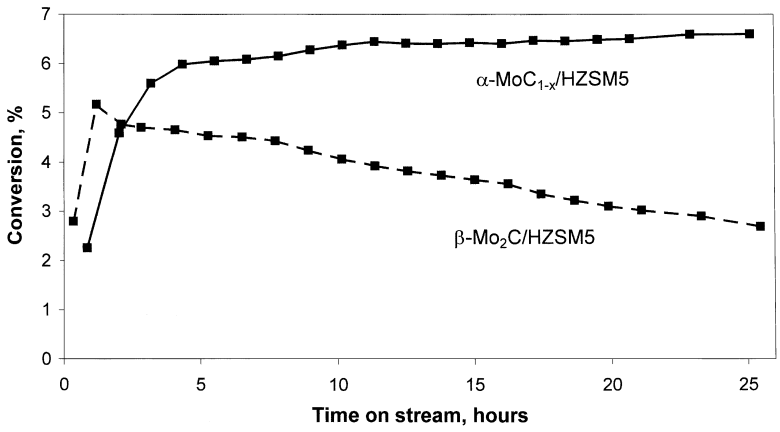

Fig. 9. Activity vs. time-on-stream of β-Mo_2C/HZSM5 and α-MoC_{1-x}/HZSM5 catalysts used for the aromatization of methane (973 K, atmospheric pressure).

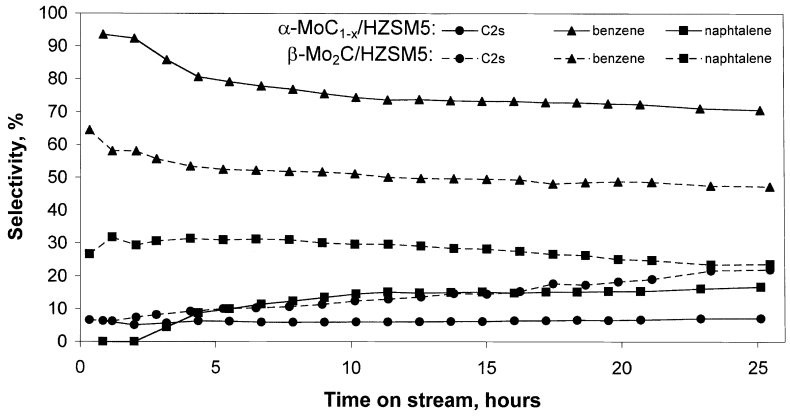

Fig. 10. Selectivity vs. time-on-stream of β-Mo_2C/HZSM5 and α-MoC_{1-x}/HZSM5 catalysts used for the aromatization of methane (973 K, atmospheric pressure).

3. Discussion

3.1. Carburization of unsupported (bulk) MoO_3

Preactivation of MoO_3 by hydrogen or a hydrogen/*n*-butane mixture at 623 K changes dramatically the nature of the molybdenum carbide, that is eventually obtained. Direct carburization of MoO_3 by methane leads to stable hcp β-Mo_2C as reported in the literature [14], whereas carburization of the pre-activated sample yields the metastable fcc carbide, α-MoC_{1-x}.

It has been demonstrated that the ⟨1 0 0⟩ direction of the fcc oxyhydride or oxycarbide phase formed at 623 K following activation under hydrogen or a hydrogen/*n*-butane mixture, respectively, is parallel to the ⟨0 1 0⟩ direction of the starting material, MoO_3 [24,25]. Thus, the formation of these fcc structures is topotactic. As the ⟨1 0 0⟩ direction of the final fcc α-MoC_{1-x} carbide obtained by carburization of the oxyhydride or oxycarbide with methane is also parallel to the ⟨0 1 0⟩ direction of MoO_3, the nature and alignment of the crystallographic system of the oxydride or oxycarbide remain unchanged during carburization (Fig. 12). The latter transformation is accompanied by an increase of a_{cub} from 0.410 to 0.428 nm, in agreement with literature data [16,24,27]. Therefore,

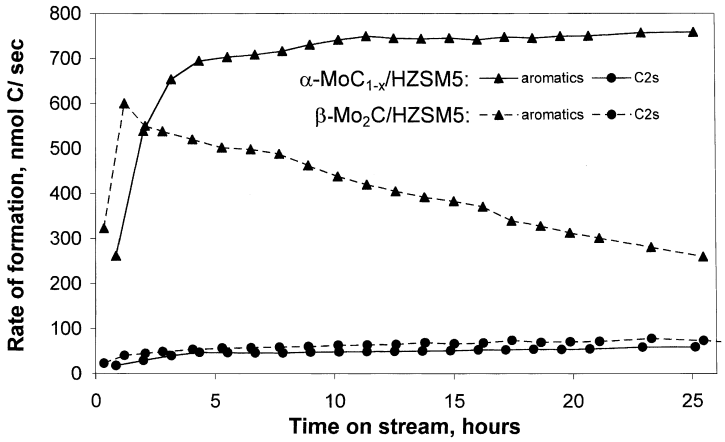

Fig. 11. Rates of formation of aromatic compounds and C_2-species vs. time-on-stream during the aromatization of methane using β-Mo_2C/HZSM5 and α-MoC_{1-x}/HZSM5 catalysts.

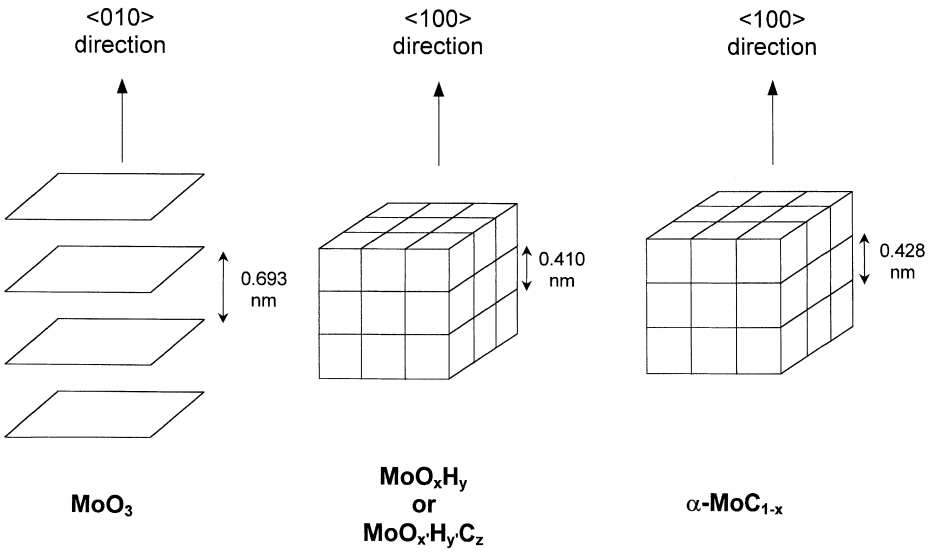

Fig. 12. Schematic representation of the activation and carburization of unsupported MoO_3. The orientation and crystallographic system of the oxyhydride or oxycarbide remain unchanged during the carburization.

it is further demonstrated that controlling the parameters of carburization (heating rate, gas mixture, space velocity, temperature, etc.) should enable the synthesis of fcc molybdenum carbides and oxycarbides of various composition. The synthesis of a molybdenum oxycarbide with $a_{\text{cub}} = 0.418\,\text{nm}$ has already been reported when using a different gas flow composition and thermal treatment (hydrogen/*n*-butane flow, $T_{\text{final}} = 823\,\text{K}$) [23].

The critical step for the formation of fcc α-MoC_{1-x} is the preliminary topotactic synthesis of a fcc structure in mild conditions, e.g. 623 K and hydrogen or a hydrogen/*n*-butane mixture. This is another illustration of Figlarz's concept about the usefulness of 'soft chemistry' applied to the synthesis of new compounds in the MoO_3–WO_3 system [30]. 'Soft chemistry' is defined as an ensemble of 'soft' chemicals operation enabling the generation of new phases by using a structural relation between the initial and final phases. In our case, the synthesis of the metastable fcc carbide involves the formation at low temperature (623 K) of a fcc structure precursor, i.e. the oxyhydride or the oxycarbide. This precursor provides oriented nucleation sites for the formation of the carbide at higher temperature. This transformation of MoO_3 must be performed at low temperature to have a preferential collapse of the MoO_3 lattice along the $\langle 0\,1\,0\rangle$ direction which corresponds to the weakest lattice energy of the oxide, without additional structural reorganizations and therefore resulting in a topotactic transformation [16].

It should, however, be emphasized that the insertion of heteroelements such as H or C into the oxide lattice can also be a critical factor promoting a topotactic transformation. Indeed, it has been shown that, in the absence of H or C insertion, the reduction of MoO_3 is not topotactic, even at 623 K [24,25]. It has also been shown that the synthesis of γ-Mo_2N from MoO_3 is topotactic because nitrogen insertion (i.e. oxynitride formation) in the solid occurs at low temperature [31]. Finally, when MoO_3 is directly carburized by methane (yielding β-Mo_2C), the intermediate phases detected are only molybdenum suboxides (Mo_4O_{11} and MoO_2), which explain why the process is not topotactic.

Interestingly, for bulk (unsupported) MoO_3, the insertion of carbon at 623 K is not mandatory. Formation of the fcc oxyhydride, MoO_xH_y, isostructural to the fcc oxycarbide, $MoO_{x'}H_{y'}C_z$, is possible. However, this does not preclude that the presence of carbon stabilizes this structure [23,32] and this effect has been demonstrated and used to synthesize fcc α-MoC_{1-x} supported on zeolite HZSM5 as discussed below.

3.2. Carburization of supported MoO_3

Calcination at 673 K is sufficient to decompose the molybdenum polymolybdates present on the dried sample after impregnation with ammonium heptamolybdate. XRD (Fig. 7) shows the presence of MoO_3 in the calcined sample, which is a prerequisite for the topotactical transformation leading to fcc α-MoC_{1-x} as discussed above.

By contrast to the bulk MoO_3 investigations reported above, treatment in hydrogen (24 h, 623 K) of HZSM5 supported molybdenum oxide obtained after calcination yields MoO_2 rather than molybdenum oxyhydride, MoO_xH_y. Treatment by a hydrogen/*n*-butane mixture results in the formation of molybdenum oxycarbide, $MoO_{x'}H_{y'}C_z$, and only traces of MoO_2. TPO of the latter sample also shows the presence of oxycarbidic carbon evolved as CO_2, which will be described elsewhere.

As the formation of zeolite-supported molybdenum oxyhydride is not observed, we conclude that the fcc structure cannot be formed in the absence of carbon. This is most likely due to the altered reducibility of supported MoO_3 compared with bulk MoO_3, as reported for MoO_3 supported on alumina [33]. It is not clear at present whether the latter is due to the smaller size of the MoO_3 crystallites or their interaction with the support.

Carburization of the sample activated under hydrogen only yields hcp β-Mo_2C/HZSM5, as expected from the presence of MoO_2 as precursor. Carburization of the sample activated under hydrogen/*n*-butane results in fcc α-MoC_{1-x}/HZSM5 as a consequence of the topotactic transformation of fcc molybdenum oxycarbide, $MoO_{x'}H_{y'}C_z$ These results agree with our observations for the bulk system.

To the best of our knowledge, it is the first time that the direct preparation of supported fcc α-MoC_{1-x} is reported. Lee et al. [38] reported that fcc α-MoC_{1-x} supported on alumina was probably formed upon carburization of molybdenum nitride, the latter resulting from the ammonia nitridation of MoO_3, but no definite characterization of the carbidic product was provided. Our results demonstrate that the critical step to obtain zeolite-supported fcc α-MoC_{1-x} is the preactivation of MoO_3 to yield a fcc molybdenum oxycarbide precursor. In the absence of a suitable hydrocarbon source, the supported fcc oxyhydride is not formed and only MoO_2 is observed. Work is currently in progress to assess if these observations and conclusions also hold for other oxidic supports.

3.3. Catalytic testing: non-oxidative conversion of methane to aromatic compounds

As seen from Figs. 9–11, the catalytic performances of the two supported carbide catalysts are significantly different.

1. β-Mo_2C/HZSM5 deactivates steadily and the conversion of methane, after 24 h, is only about 50% of the maximal conversion (5.2%) observed after 2 h (Fig. 9). By contrast, no deactivation is observed for α-MoC_{1-x}/HZSM5, even after 24 h on stream (Fig. 9), and a *stable* methane conversion of 6.7 % is maintained at a level comparable or superior to that reported by other authors [19,20,34–37] for *deactivating catalysts*. It should also be noted that the maximum conversion of methane to aromatic compounds at 973 K is about 11% as governed by thermodynamics.
2. The benzene/naphthalene ratio in the products, expressed on a carbon basis, is about 2 for β-Mo_2C/HZM5 and 4 for α-MoC_{1-x}/HZSM5, and these ratios are maintained throughout the whole catalytic runs (Fig. 10). Thermodynamics predict that benzene and naphthalene should be produced in nearly equimolar amounts at 973 K and thus their thermodynamic ratio expressed on a carbon basis should be about 0.6.
3. The rate of aromatic compounds formation, on a carbon basis, follows the trends observed for the methane conversion for both catalysts (Fig. 11). C_2-species (ethane and ethylene) are formed at a lower rate on α-MoC_{1-x}/HZSM5 compared with β-Mo_2C/HZSM5 and after a few hours on stream, these rates remain constant for both catalysts.

Deactivation of the catalyst at 973 K could be due to either modifications occurring in the zeolite or the molybdenum carbide, or to coke deposition on the catalyst. We did not obtained evidence for structural modifications and we therefore conclude that coke deposition is responsible for the deactivation of β-Mo_2C/HZM5, compared with previous reports. The latter conclusion is substantiated by the observation that α-MoC_{1-x}/HZSM5 is less selective to naphthalene and has a lower ethane

formation rate than β-Mo_2C/HZM5, remembering that naphthalene is obviously a coke precursor and that more saturated light alkane species are likely to be formed by hydrogen transfer reaction when coke deposition occurs. One should also remember that di-alkylation of benzene by ethylene in adjacent positions leads to a di-ethylbenzene naphthalene and coke precursor, a reaction which appears to be less likely on α-MoC_{1-x}/HZSM5. These proposals are substantiated by TPO results showing that used β-Mo_2CIHZM5 catalysts contains mostly 'hard' (most probably polyaromatic) coke located at the zeolite external surface, considering molecular shape selectivity effects, likely to block the zeolite pore mouths and cause deactivation whereas the 'used' α-MoC_{1-x}/HZSM5 catalyst is essentially contaminated by 'soft' coke probably C_2 oligomers) partially occupying the intracrystalline volume of the zeolite [21]. The formation of 'soft' coke on α-MoC_{1-x}/HZSM5 certainly indicates that light olefinic species are involved as intermediates in the methane dehydrocyclization reaction.

The higher benzene to naphthalene ratio, relative to thermodynamic predictions, can be explained by considering the well-known molecular shape selectivity effects which are imposed by intermediate pore size zeolite catalysts. However, we have no firm explanation at this point to rationalize the higher benzene to naphthalene ratio observed for α-MoC_{1-x}/flZSM5 relative to its β-Mo_2C/HZM5 counterpart. Zeolite steric (molecular shape selective) constraints being identical for both catalysts, this difference can be due to either a different localization or dispersion of the α and β molybdenum carbides in or on the zeolite, as different protocols were followed for their preparation, or to intrinsic differences in the catalytic activities. In the latter respect, it is worth noting that the rate of benzene formation is higher on α-MoC_{1-x}/HZSM5. The α-MoC_{1-x} metastable phase may be more prone to activate methane than the stable β-Mo_2C phase.

As mentioned above, we have no firm explanation for the higher selectivity of the α-MoC_{1-x}/HZSM5 catalyst towards benzene. We hypothesize, however, that it is due to a higher pore mouth blockage, resulting from 'hard' coke deposition at the external surface of HZM5, for the β-Mo_2C/HZM5 catalyst, leading to product molecular shape selectivity effects. This may imply that β-Mo_2C species could be located essentially at the external surface of the HZSM5 crystals whereas (part of) α-MoC_{1-x} or other Mo-containing species resulting from the hydrogen/*n*-butane preactivation treatment might also be located in the zeolite intracrystalline volume. We are currently exploring this possibility and do not exclude, however, that the α and β molybdenum carbides may have different catalytic behaviors for the aromatization of methane, as differences in their catalytic performance as shown already [11].

Our results demonstrate the importance of controlling the conditions for the formation of the desired supported molybdenum carbides (fcc or hcp) phases and show how the catalytic properties of HZSM5 supported Mo carbide catalysts can be affected. Additional work, in progress, is needed to ascertain whether different catalytic behaviors are due to the nature of the molybdenum carbide phase, its location, and/or its dispersion.

4. Conclusions

The initial topotatic transformation of MoO_3 to the fcc molybdenum oxyhydride or oxycarbide in 'soft' conditions, as achieved at 623 K using hydrogen or a hydrogen/*n*-butane mixture, is a prerequisite for the synthesis of fcc α-MoC_{1-x} by further carburization of these phases with methane at higher temperature.

In contrast to bulk MoO_3, MoO_3 supported on HZM5 is only converted to fcc α-MoC_{1-x} when preactivation is achieved with a hydrogen/*n*-butane mixture. The reducibility of MoO_3 is affected by the zeolite support and carbon insertion in the oxidic phase is necessary to stabilize the fcc structure.

The preparation of HZSM5 supported fcc molybdenum carbide, α-MoC_{1-x}, has been achieved successfully via the above route. It is proposed that this carbon insertion and fcc structure stabilization method may be a generic route for the preparation of fcc α-MoC_{1-x} on various oxidic supports.

Hcp β-Mo_2C, prepared by direct carburization of MoO_3 with methane, and fcc α-MoC_{1-x}, prepared as mentioned above, both supported on HZSM5, have very different catalytic properties for the non-oxidative conversion of methane to aromatic compounds at 973 K. Fcc α-MoC_{1-x} has superior performance,

showing a higher methane conversion, a higher selectivity to benzene, and no deactivation after 24 h on stream.

Acknowledgements

J.R.A. and C.B. thank EPSRC for financial support, a quota studentship and EPSRC Grant GR/M71794, respectively. I.S. acknowledges financial support from ATV Denmark, under its Danish Industrial PhD scheme. All authors are also grateful to Haldor Topsøe A/S for additional support.

References

[1] R.B. Levy, M. Boudart, Science 181 (1973) 547.
[2] S.T. Oyama, The Chemistry of Transition Metals Carbides and Nitrides, Blakie, London, 1996, p. 1.
[3] P.W. Lednor, Catal. Today 15 (1992) 243.
[4] S.T. Oyama, G.L. Haller, Surface and Defect Proportion of Solids, Vol. 5, Chemical Society, London, 1982, p. 333.
[5] L. Leclerq, in: J.P. Bonnelle, D. Delmon, E.G. Derouane (Eds.), Sufface Properties and Catalysis by Non-Metals, NATO ASI Series, 1983, p. 433.
[6] M.J. Ledoux, C. Pham-Huu, J. Guille, H. Dunlop, S. Marin, M. Weibel, Catal. Today 15/2 (1992) 263.
[7] J.S. Lee, M. Boudart, Appl. Catal. 19 (1985) 207.
[8] E.J. Markel, J.W. Van Zee, J. Catal. 126 (1990) 643.
[9] J.G. Choi, J.R. Brenner, L.T. Thomson, J. Catal. 154 (1995) 33.
[10] S. Li, J.S. Lee, T. Hyeon, K.S. Suslick, Appl. Catal. 184 (1999) 1.
[11] G.S. Ranhotra, A.T. Bell, J.A. Reimer, J. Catal. 108 (1987) 40.
[12] D.J. Sajkowski, S.T. Oyama, Appl. Catal. 134 (1996) 339.
[13] F. Solymosi, R. Nemeth, Catal. Lett. 62 (1999) 197.
[14] J.S. Lee, S.T. Oyama, M. Boudart, J. Catal. 106 (1987) 125.
[15] L. Volpe, M. Boudart, J. Solid State Chem. 59 (1985) 348.
[16] J.S. Lee, L. Volpe, F.H. Ribeiro, M. Boudart, J. Catal. 112 (1988) 44.
[17] C. Bouchy, S.B. Derouane-Abd Hamid, E.G. Derouane, Chem. Commun. 2 (2000) 125.
[18] E. Segal, I. Ivanova, E.G. Derouane, Rev. Roum. Chimie 38 (1993) 1127.
[19] L. Wang, L. Tao, M. Xie, G. Xu, J. Huang, Y. Xu, Catal. Lett. 21 (1993) 35.
[20] D. Wang, J.H. Lunsford, M.P. Rosynek, J. Catal. 169 (1997) 347.
[21] S.B. Derouane-Abd Hamid, J.R. Anderson, I. Schmidt, C. Bouchy, C.J.H. Jacobsen, E.G. Derouane, Catal. Today, submitted for publication.
[22] P. Del Gallo, C. Pham-Huu, C. Crouzet, M.J. Ledoux, Ind. Eng. Chem. Res. 36 (1997) 4166.
[23] C. Bouchy, C. Pham-Huu, B. Heinrich, C. Chaumont, M.J. Ledoux, J. Catal. 190 (2000) 92.
[24] C. Bouchy, PhD thesis, Umversité Louis Pasteur, Strasbourg, 1998.
[25] C. Bouchy, C. Pham-Huu, M.J. Ledoux, Appl. Catal. A, submitted for publication.
[26] C. Bouchy, C. Pham-Huu, B. Heinrich, E.G. Derouane, S.B. Derouane-Abd Hamid, M.J. Ledoux, in preparation.
[27] I.F. Ferguson, J.B. Ainscough, D. Morse, A.W. Miller, Nature 202 (1964) 1327.
[28] E. Rudy, S. Windisch, A.J. Stosick, J.R. Hoffman, Trans. TMS-AIME 239 (1967) 1247.
[29] H.R. Oswald, J.R. Günter, in: E. Kaldis, H.J. Scheel (Eds.), Crystal Growth and Materials, North-Holland, Amsterdam, 1977.
[30] M. Figlarz, Prog. Solid State Chem. 19 (1989) 1.
[31] L. Volpe, Ph.D. thesis, Stanford University, 1985.
[32] P. Delporte, C. Pham-Huu, M.J. Ledoux, J. Chim. Phys. 93 (1996) 507.
[33] C. Pham-Huu, P. Del Gallo, E. Peschiera, M.J. Ledoux, Appl. Catal. A 132 (1995) 77.
[34] D. Wang, M. Rosynek, J.H. Lunsford, Topics Catal. 3 (1996) 289.
[35] F. Solymosi, A. Szoke, J. Cserenyi, Catal. Lett. 39 (1996) 157.
[36] H. Juang, L. Wang, W. Cui, Y. Xu, Catal. Lett. 57 (1999) 95.
[37] R. Ohnishi, S. Liu, Q. Dong, L. Wang, M. Ichikawa, J. Catal. 182 (1999) 92.
[38] J.S. Lee, H.K. Lee, J.Y. Lee, J. Phys. Chem. 96 (1992) 362.